

A non-hydrostatic numerical model for calculating of free-surface stratified flows in the coastal sea

YULIYA KANARSKA, VLADIMIR MADERICH (*Institute of Mathematical Machine and System Problems, Glushkova av. 42, 03187 Kiev, Ukraine, kanarska@ukrpost.net*)

1 Introduction

The non-hydrostatic effects are important in a wide spectrum of stratified flows in the coastal seas. The examples are the buoyant plumes from submerged outfalls, internal waves of large amplitude generated by the tidally driven flows over a steep topography and exchange flows over the sills in the sea straits. In this paper a three-dimensional numerical model for simulation of the free-surface stratified flows in the coastal sea is presented. The model is a non-hydrostatic extension of free-surface primitive equation POM model with vertical sigma-coordinate (*Blumberg and Mellor* [1987]). The pressure field was decomposed on hydrostatic and non-hydrostatic components. The model equations were integrated with mode splitting technique and four-stage procedure, where the level was determined at first. The hydrostatic, non-hydrostatic components of pressure, velocity and scalar fields were calculated at subsequent stages. Unlike the most of non-hydrostatic models 2D depth-integrated momentum and continuity equations were integrated explicitly at first stage, whereas 3D equations were solved implicitly at rest stages. This approach is particularly advantageous for the shallow stratified flows and is fully compatible with the POM model.

The model was tested against laboratory experiments check its ability to reproduce local scale non-hydrostatic phenomena in coastal sea. The surface solitary wave interaction with the vertical wall, the formations of solitary «bulges» in thin pycnocline as the result of the collapse of mixed region and water exchange through strait are considered.

2 Model Descriptions

The model is based on the 3D Reynolds-averaged Navies-Stokes equations for Boussinesq fluid. The concept of eddy viscosity and diffusivity is used with two-equation model of turbulence model to define turbulent stresses and scalar fluxes. The sigma-coordinate system for the vertical direction is used. The pressure and velocity fields are decomposed on hydrostatic and non-hydrostatic components. The mode splitting technique (*Blumberg and Mellor* [1987]) for external and internal modes was applied. The finite-difference solutions of governing equations were derived using four-stage procedure:

1 stage: Free surface level.

The calculation of free surface elevation is performed by explicit method from depth-integrated shallow water equations like the POM model. The initial 2D velocity fields on each external stage is determined by direct integrating of general non-hydrostatic 3D velocity fields from previous internal step.

2 stage: Hydrostatic components of velocity and pressure.

The 3D hydrodynamic equations without non-hydrostatic pressure are solved with internal time step semi-implicitly (*Casulli and Stelling* [1998]) to determine provisional values of velocity. The advection, horizontal viscosity and diffusion were discretized explicitly. The obtained three-diagonal system is solved by a direct method.

3 stage: Non-hydrostatic components of velocity and pressure.

The non-hydrostatic components of velocity are computed by correcting the provisional velocity

field with the gradient of non-hydrostatic pressure to satisfy continuity equation for sum of hydrostatic and non-hydrostatic velocity. The obtained discretized Poisson equation for the non-hydrostatic pressure reduced to the non-symmetric 15 diagonal linear system, part of which arise from the sigma-transformation components. The preconditioned biconjugate gradient method is used for solving this system. Once the non-hydrostatic pressure is determined the corresponding components of velocity fields are calculated.

4 stage: Scalar fields.

The scalar fields (temperature and salinity, turbulent quantities) are computed by using semi-implicit numerical scheme in vertical direction. The obtained three-diagonal system is solved by a direct method.

3 Numerical Application and discussion

Impact of solitary surface wave on vertical wall. Here, results of a computation are compared with the laboratory experiments on solitary surface wave interaction with a vertical wall in the wave flume with depth H . As seen in Fig. 1, the model predicted well maximum of elevation η at the wall. The time dependence of wave pressure on undisturbed surface p is shown in Fig. 2. Non-hydrostatic model reproduced quite well observed in experiments characteristic two-peak profile of pressure with depression near to the moment of maximum runoff that was caused by the vertical acceleration of fluid at the wall.

Propagation of intrusive "bulge" in the pycnocline. The second example concerned with the formation and evolution of large amplitude intrusive "bulge" that was generated by collapse of mixed region in the thin pycnocline. The results of simulation are compared in Fig. 4 with experiment 302 of Maderich *et al.* [2001] that was conducted in the tank $6.7 \times 0.4 \times 0.19$ m. The tank was filled with two homogeneous layer of different salinity. The circular mixed region with diameter 0.19 m collapsed in the centre of tank. The resulted solitary bulges (compare Fig. 4 and 5) moved with almost constant speed that exceeded values, predicted by theory of weakly nonlinear long internal waves.

Exchange flows through long straits with sill. Here, the exchange flow through shallow and narrow strait connected two deep and wide basins filled by water of different density is considered. The laboratory experiment 701 (Maderich [2000]) was simulated. The strait is rectangular with length $L=60.5$ cm, maximal depth $H=8$ cm and constant width $A=0.9$ cm. The sill with $h/H=0.5$ is placed in the centre. The buoyancy difference is $g\Delta\rho/\rho=1.48$ cm/c². This difference was maintained by heating of left basin and cooling of right one. The exchange in the strait is maximal. The sill together with right end of strait hydraulically control the exchange, whereas only flow in the lower layer is critical at left end of the strait. The flow is laminar, however, measurements showed broadening of thermocline at the left side of sill (see Fig. 6). The computations by non-hydrostatic model were carried out with laminar viscosity and conductivity and resolution $250 \times 8 \times 100$. The internal and external time step were 0.015 s and 0.001 s. The simulated density distribution also showed difference between thickness of interface on both sides of sill (see Fig.7). The detailed investigation of velocity field in Fig.8 shows presences of complicated flow structure at left side of the sill. The supercritical flow slows down in the point of internal hydraulic jump that causes countercurrent. It lifts dense water along the left side of sill and turns finally to left, forming broad interface layer. The broadening of pycnocline downstream of sill or contraction was frequently observed in the sea straits, however, it was attributed to the turbulent mixing only. The comparison of non-hydrostatic and hydrostatic calculations was carried out with the same resolution. Fig.9 indicates essential contribution of nonhydrostatic components at the slope and foot of the sill with the difference in velocities about 20%. Non-hydrostatic calculations is stable for high resolution, whereas hydrostatic calculations was unstable for the same internal step and requires to reduce internal step by one half.

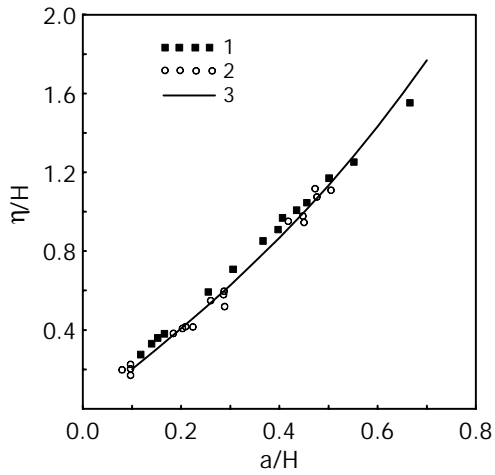


Figure 1: Runup on the vertical wall as a function of soliton height as measured by *Maxworthy* [1979] (1), *Zagriadskaya and Ivanova* [1978] (2) and calculated (3).

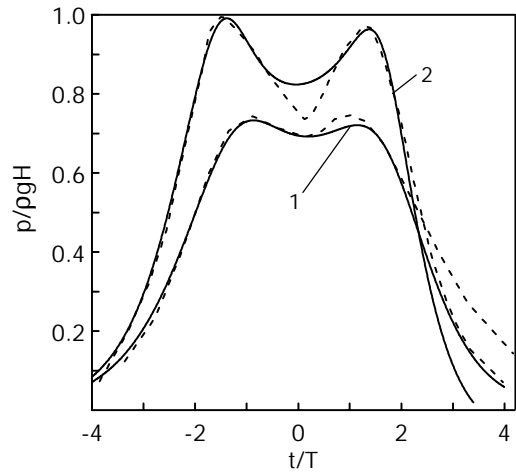


Figure 2: Time dependence of wave pressure for dimensionless soliton height $a/H = 0.5$ (1) and 0.7 (2). Solid line is simulation and dash line is experiment (*Zagriadskaya and Ivanova* [1978]).

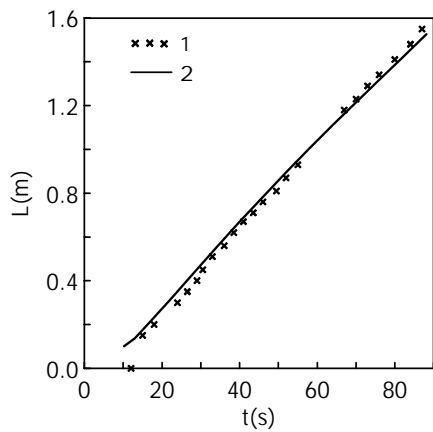


Figure 3: Intrusion length as a function of time in experiment 302 (*Maderich et al.* [2001]) (1) and calculated (2).

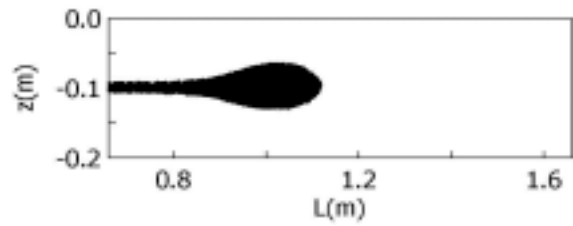


Figure 4: Computed intrusion visualized with markers.



Figure 5: Dye-visualized intrusion in experiment 302.

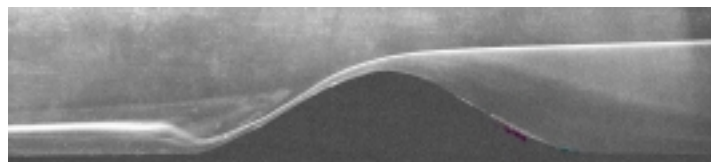


Figure 6: Photo of experiment 701 (*Maderich* [2000])

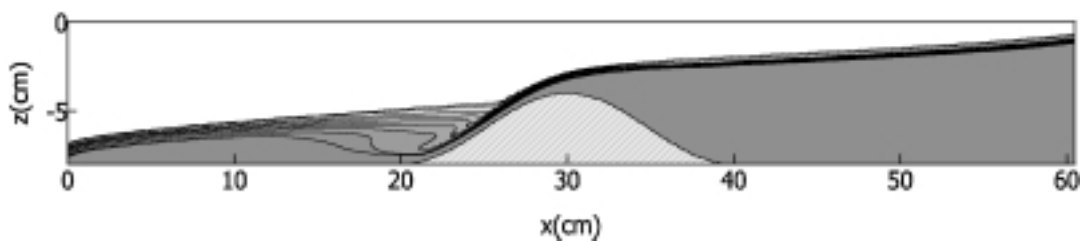


Figure 7: Computed density distribution for experiment 701.

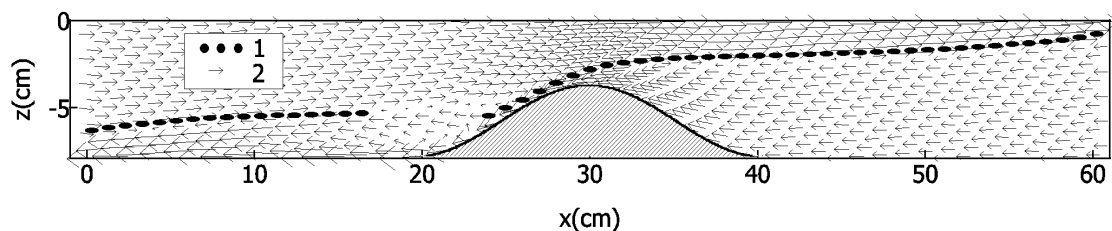


Figure 8: Interface position in experiment 701 (1) and non-hydrostatic velocity field (2).

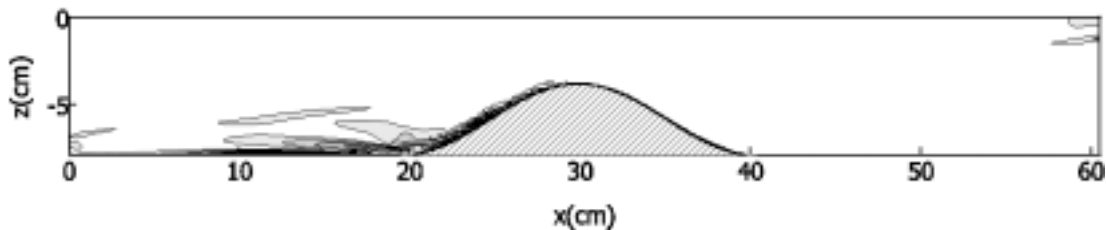


Figure 9: Module of difference between hydrostatic and non-hydrostatic velocity fields

4 Conclusions

The non-hydrostatic model for simulating of free-surface stratified flows in the coastal sea has been developed. The numerical algorithm is a non-hydrostatic extension of POM model and fully compatible with it. Several oceanographically motivated examples of non-hydrostatic currents were considered. They demonstrate the effectiveness of this tool for wide spectrum of coastal sea problems.

Acknowledgments: This study was partially supported by CRDF project “Improved methodology for assessing the impacts of the Aegean-Black Sea exchange”.

References:

Blumberg, A.F. and Mellor, G.L. A description of a three-dimensional coastal ocean circulation model, in N.S. Heaps (ed.), *Three-Dimensional Coastal Ocean Circulation Models, Coastal and Estuarine Sciences*, vol. 4, AGU, Washington, DC, 1987, pp. 1–16.

Casulli V., Stelling G. S., Numerical simulation of 3D quasi-hydrostatic, free-surface flows. *J. Hydr. Eng.*, 124, 678-686, 1998.

Maderich V. S., Two-layer exchange flows through long straits with sill. *Oceanic Fronts and Related Phenomena. Konstantin Fedorov Int. Memorial Symp., IOC Workshop Rep. Series*, N 159, UNESCO’2000, 326-331, 2000.

Maderich, V., van Heijst, G.J., Brandt, A. Laboratory experiments on intrusive flows and internal waves in a pycnocline. *J. Fluid Mech.*, 432, 285-311, 2001.

Maxworthy T., Experiments on collisions between solitary waves. *J. Fluid. Mech.*, 76, 177—185, 1976.

Zagriadskaya N. N., Ivanova S. V. Action of long waves on the vertical obstacle. *Izv. VNIIG*, 138, 94-101, 1988.